Phase behavior of a simple model for membrane proteins

Massimo G. Noro[a] and Daan Frenkel
FOM Institute for Atomic and Molecular Physics, Kruislaan 407, 1098 SJ Amsterdam, The Netherlands

(Received 15 September 2000; accepted 14 November 2000)

We report a numerical simulation of the phase diagram of a simple model for membrane proteins constrained to move in a plane. In analogy with the corresponding three-dimensional models, the liquid–gas transition becomes metastable as the range of attraction decreases. Spontaneous crystallization happens much more readily in the two-dimensional models rather than in their three-dimensional counterparts. © *2001 American Institute of Physics.*
[DOI: 10.1063/1.1338504]

I. INTRODUCTION

If one picture is worth a thousand words, recent advances in x-ray crystallography are providing the equivalent of a dictionary. Crystallographers are now solving the three-dimensional structure of proteins at the rate of one or more per day. A bottleneck is the difficulty of growing high-quality crystals for x-ray analysis.

As the success of protein crystallization depends strongly on the physical conditions of the initial solution,[1,2] much effort has gone into finding the relation between solvent conditions and crystallization behavior. Rosenbaum *et al.*[3] analyzed the solubility curves of a variety of globular proteins and found that they can be made to superimpose when expressed in appropriate scaled units. What this suggests is that the phase behavior of many globular–protein solutions obeys a law of corresponding states. Specifically, they showed that the solid–fluid phase boundary of the proteins in solutions can be mapped onto the corresponding curve of a simple model system (the hard-core Yukawa potential[4]) with short-ranged attractions. Such corresponding states behavior suggests that — for a given class of compounds — the solubility boundary is only weakly dependent on the details of the interaction potential.

Far fewer crystals have been grown of membrane proteins than of globular proteins. The reason is simply that it is more difficult to crystallize membrane proteins than globular proteins. It would, of course, be very interesting to know if the ''generic'' features of the phase behavior of quasi-two-dimensional proteins are similar to those of globular proteins. It is tempting to start such an analysis by looking at the corresponding ''minimal'' model for membrane proteins—namely, one of circular disks with isotropic, short-ranged attractive interactions. In this paper, we report a numerical study of the phase behavior of such model membrane proteins. In our study, we vary the range of the attractive interaction between the particles. We find that the general topology of the phase diagram is indeed similiar to that for three-dimensional (''globular'') proteins. In particular, we find that the liquid-vapor transition is preempted by the freezing curve for particles with sufficiently short-ranged attractions. However, quantitatively, there are large differences. In contrast to the three-dimensional case which still exhibits a well-defined metastable liquid–vapor coexistence curve below the equilibrium freezing curve, we find crystallization, rather than fluid–fluid demixing, in the corresponding ''membrane-protein'' model.

II. MODEL

We model the effective interaction between membrane proteins using an extension of the well-known Lennard-Jones potential,

$$v(r)=\begin{cases}\infty, & r\leqslant\sigma,\\ \dfrac{4\epsilon}{\alpha^2}\left(\dfrac{1}{[(r/\sigma)^2-1]^6}-\dfrac{\alpha}{[(r/\sigma)^2-1]^3}\right), & \sigma<r,\end{cases} \tag{1}$$

where σ denotes the hard-core diameter of the particles and ϵ the well depth. The width of the attractive well can be adjusted by varying the parameter α: the smaller α the longer the range of attractions. Figure 1 plots this potential for the values of α used in this paper. Note that as α decreases, the range of repulsions increases as well, so that the ''effective'' size of the particle grows. It is, however, convenient to compare the simulation results for particles that have the same hard-core diameter. To estimate the effective hard-core diameter for a given value of α, we separate the potential into an attractive v_{att} and a repulsive v_{rep} contribution in the spirit of the Weeks–Chandler–Andersen method.[5] We then calculate the equivalent hard-core size of the repulsive part of the potential using the Barker–Henderson criterion,[6]

$$\sigma_{\mathrm{eff}}=\int_0^\infty dr[1-e^{-v_{\mathrm{rep}}(r)/k_BT}]. \tag{2}$$

In what follows, we use α_{eff} as our unit of length. In these units, all our model proteins have the same effective diameter.

[a]Present address: Unilever Research Port Sunlight, Quarry Road East, Bebington Wirral CH633JW, United Kingdom. Electronic mail: Massimo.Noro@Unilever.com

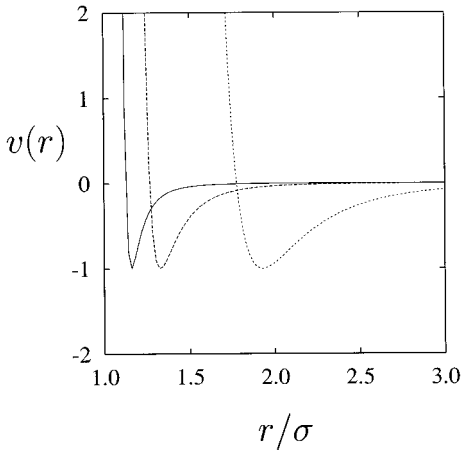

FIG. 1. Interaction potential and defined in Eq. (1) corresponding to $\alpha=50$ (—), $\alpha=4.5$ (– – –), and $\alpha=0.1$ (---). Note that as α decreases, attractions become longer ranged but the range of repulsions increases as well, so that the ''effective'' size of the particle grows. (We have set $\epsilon=1$.)

III. COMPUTATIONAL METHODS

In order to map out the phase diagram of our two-dimensional model for membrane proteins, we have used a combination of simulation techniques that we discuss briefly in this section.

A. Gibbs–Duhem integration

This method was proposed by Kofke,[7,8] and is based on the integration of the Clausius–Clapeyron equation, which expresses the slope of the phase boundary in the (P,β) diagram,

$$\frac{dP}{d\beta}=-\frac{\Delta h}{\beta\Delta v}, \tag{3}$$

where $\beta=1/k_BT$, P is the pressure, Δh and Δv are the differences in enthalpy and volume (per particle) in the two coexisting phases, respectively. To compute this slope, two simulations are carried out in parallel: one in the liquid phase and one in the solid. The two systems are held at the same temperature and pressure, but cannot interact with each other; during the runs we measure the average density $(1/v)$ and enthalpy h per particle and thus determine $(dP/d\beta)$. Knowing this slope, we can then estimate the location of a neighboring point on the (P,β) coexistence curve. The Gibbs–Duhem method is straightforward, but there are several ways in which it can be implemented, and there are several subtleties that require attention.

The first is the choice of a good starting point. The Gibbs–Duhem integration method allows one to trace out the (P,β) coexistence curve once one point on this curve is known. There are several ways to select this point. In one set of calculations, we started the stepwise integration at $\beta=0$ (i.e., the infinite temperature limit) where the phase diagram approaches that of hard disks. Here we have used the fluid–solid equilibrium density gap reported by Jaster[9] as the input of our first Gibbs–Duhem simulation. However, as the freezing transition of hard disks is itself still not completely characterized,[10] this is not necessarily the best option. In fact independent free-energy calculations allow us to start the Gibbs–Duhem integration at a finite value of β where we find a strong first-order liquid–solid phase transition. We found this second route more reliable.

The second point is the choice of the form of the equation to be integrated. The Gibbs–Duhem method is not self-correcting. This means that small numerical errors may cause the computed coexistence curve to diverge from the true phase-equilibrium curve. To minimize this problem, the right-hand side of Eq. (3) must be a smooth function of pressure and temperature, so that simple integration schemes can be applied with high accuracy. In our case we found that at high temperatures a suitable slowly varying function was

$$\frac{d\log P}{d\log\beta}=-\frac{\Delta e+P\Delta v}{P\Delta v}, \tag{4}$$

where Δe is the difference in the energy per particle between the two coexisting phases. In the hard-particle limit the $P\Delta v$ term completely overwhelms the energy difference, and the slope of the phase boundary plotted in the $(\log P,\log\beta)$ diagram approaches -1. We have verified this in our simulations. In the low temperature regime the most convenient differential form of the Clausius–Clapeyron equation, in agreement with Kofke[7] and Hagen,[4] was found to be

$$\frac{d\log\beta P}{d\beta}=-\frac{\Delta e}{\beta P\Delta v}. \tag{5}$$

Equations (4) and (5) were solved using a second-order predictor-corrector algorithm. As such algorithms are not self-starting, we initiated the integration by supplying the values of the integrand and its slope (when known), and using a first-order algorithm for the prediction of the first point; after two integration steps we continued with the desired second order procedure. In Fig. 2 we collect the phase transition points obtained from numerical integration of Eqs. (4) and (5).

The third point has to do with spontaneous phase transitions during a single phase simulation. In two dimensions there is much less hysteresis in the solid–liquid transition than in three dimensions. As a consequence, it may happen that, in a constant-pressure simulation of a relatively small system (in our case, $N=256$), a fluid could *spontaneously* transform into a solid, or vice versa. This creates a problem for the Gibbs–Duhem simulations that involve constant-pressure studies of state points along the solid–fluid coexistence line. To prevent such undesirable (and, on a macroscopic scale, irrelevant) fluctuations, we imposed a constraint on the degree of crystallinity of the system. The degree of crystallinity was measured using a global bond-order parameter.[11] If during a constant-pressure Monte Carlo simulation of the liquid (or solid) phase, the value of the bond-order parameter of a configuration was outside the interval typical for the phase under consideration, then the configuration was rejected. Typically no more than 0.5% of the configurations were rejected during a simulation of any state point.

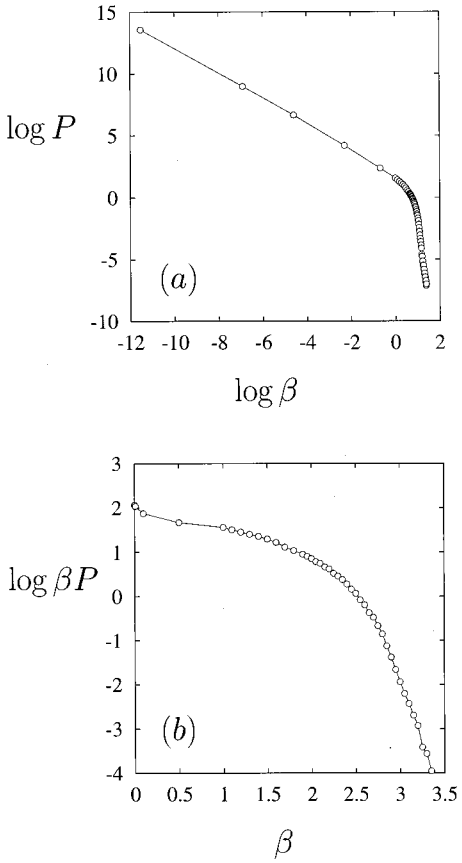

FIG. 2. Phase boundary in the two representations used for the Gibbs–Duhem integration scheme. (a) In the high temperature regime and (b) in the low temperature regime.

B. Thermodynamic integration

Thermodynamic integration is the method most commonly used to locate the solid–liquid transition. The procedure involves the comparison of the chemical potentials of the liquid and solid phases at equal temperature and pressure. The result of such a calculation is a (μ,P)-diagram similar to the one shown in Fig. 3. Two phases are in equilibrium at the point where the two chemical potential curves cross. Evaluation of the chemical potential of the fluid branch is straightforward once the equation of state of the fluid is known from low densities up to the density range of interest. In the present case, we did this by performing a large number of NPT-Monte Carlo simulations at different state points (see Fig. 4). We then fitted the numerical data for the pressure to a convenient fitting function. In the present case, we used an ad hoc generalization of the so-called *y*-expansion that is often used to describe the equation of state of hard-body fluids,[12]

$$\beta P=\frac{\rho}{1-a\rho}+b\left(\frac{\rho}{1-a\rho}\right)^2+c\left(\frac{\rho}{1-a\rho}\right)^3, \tag{6}$$

where *a*, *b*, and *c* are to be determined from the fit. Upon integration of the pressure (6) between zero density (ideal gas limit) and the density of interest, one obtains an explicit expression for the chemical potential,

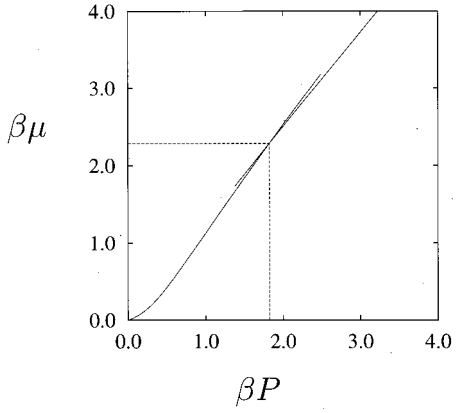

FIG. 3. Plot of the chemical potential μ as a function of the pressure P for the liquid and the solid phase. The transition condition is satisfied at the crossing; at a fixed temperature the chemical potentials and the pressure are equal. Here we neglect the de Broglie wavelength contribution. The calculation equilibrium pressure does not change since one subtracts the same quantity, namely, $\ln \lambda^2$, from the chemical potential of both phases.

$$\beta\mu(\rho)=\ln\frac{\rho\Lambda^2}{1-a\rho}+\frac{b/a-c/a^2+1}{1-a\rho}+\frac{c/2a^2+b\rho}{(1-a\rho)^2}+\frac{c\rho^2}{(1-a\rho)^3}-(b/a-c/2a^2+1), \tag{7}$$

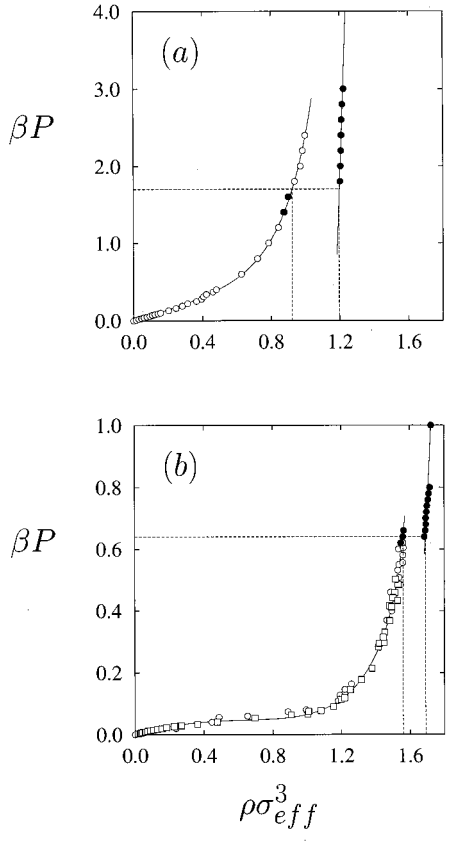

FIG. 4. Equation of state, or (P,ρ)-isotherm, calculated at the same temperature for two different ranges of interactions: (a) extremely short (α=50), (b) extremely long (α=0.1). The simulation data have been collected by measuring the average density in NPT-Monte Carlo simulations when compressing a liquid (○) or when expanding a solid (●), and (□) measuring the average pressure in μVT-Monte Carlo simulations.

where Λ is the de Broglie wavelength. In the case of the solid phase, we fit the calculated (P,ρ)-isotherms to a simple power law of the form $a\rho^2+b\rho+c$. Integrating between a reference density ρ^* and the present density yields the chemical potential

$$\beta\mu(\rho)=2a\rho+b(\ln\rho+1)-(a\rho^*+b\ln\rho^*-c/\rho^*)+\beta f^{*\mathrm{ex}}(\rho^*)+\ln\Lambda^2\rho^*-1, \quad (8)$$

where $f^{*\mathrm{ex}}(\rho^*)$ is the excess Helmholtz free energy per particle evaluated at the reference density ρ^*. A method that is widely used to compute the free energy of a crystalline solid is the so called ''Einstein crystal'' method proposed by Frenkel and Ladd,[13] which employs thermodynamic integration of the Helmholtz free energy along a reversible artificial path between the system of interest and an Einstein crystal. The Einstein system is used as a reference since there is a simple analytical expression for its partition function, which allows a determination of the *absolute* value of its free energy. We typically performed a series of 10 NVT-simulations at the reference density ρ^*, switching gradually from the Einstein crystal to our system of interest, by modifying the value of the coupling constant λ, where $\lambda=1$ corresponds to the Einstein crystal and $\lambda=0$ to the system of interest. The value of the excess free energy takes a simple form,[14]

$$\beta f^{*\mathrm{ex}}(\rho^*)=-\frac{d}{2}\ln\left[\frac{2\pi}{\alpha\beta}\right]+\frac{\beta U_0}{N}-\frac{\beta}{N}\int_0^1 d\lambda\langle\Delta U\rangle_\lambda-\frac{N-1}{N}\ln\rho+1-\frac{d+1}{2N}\ln N-\frac{1}{2N}\ln 2\pi, \quad (9)$$

where d is the dimensionality, N is the size of the system, α is the spring constant of the Einstein crystal, and U_0 the potential energy of the crystal with all the atoms in their lattice positions. The difference between the energy of the Einstein crystal and that of the system of interest, $\Delta U \equiv U_{\mathrm{Ein}}-U$, enters in the third term in Eq. (9) and the integral in this term is evaluated numerically as explained in Ref. 15.

Once the transition pressure is known, from the crossing of the two chemical potential curves of Fig. 3, one simply reads off the coexisting densities from the (P,ρ) diagram. In Fig. 4 we show two typical equations of state for the case $\alpha=50$ and $\alpha=0.1$ where we have collected state points using both NPT-simulations and μVT-simulations (i.e., performed in the Grand Canonical Ensemble). At low temperatures it becomes increasingly difficult to equilibrate the fluid system, especially if the series of simulations is performed as a gradual compression. The occasional formation of high density clusters of particles generates locally a highly incompressible fluid, and a typical compression move is therefore very unlikely to succeed. On the other hand, by keeping the chemical potential constant, the density can be more easily increased by adding new particles. The transition calculated via the thermodynamic integration route is completely consistent with our simulation data, and the transition is predicted to fall inside the observed ''hysteresis'' loop.

TABLE I. Coexistence data for the liquid–gas equilibrium. β is the inverse temperature and ρ is the number density. The uncertainties $\Delta\rho$ quoted here refer to the half-width of the histogram indicating the probability of finding a certain density during the simulation. By fitting ρ_{gas} and ρ_{liq} to the law of rectilinear diameters, we extrapolate the critical point at $\beta_c=2.392$ and $\rho_c=0.134$.

β	ρ_{gas}	$\Delta\rho$	ρ_{liq}	$\Delta\rho$
2.60	0.015	0.010	0.250	0.005
2.55	0.020	0.010	0.245	0.005
2.525	0.020	0.010	0.240	0.010
2.50	0.0225	0.010	0.235	0.010
2.475	0.020	0.015	0.230	0.015
2.45	0.032	0.015	0.228	0.010
2.425	0.040	0.020	0.230	0.020
2.40	0.060	0.015	0.220	0.015
2.375	0.070	0.020	0.200	0.020
2.35	0.090	0.020	0.180	0.020

We have verified the computed (μ,P)-curves of the fluid, by calculating independently the chemical potential, using the Widom particle-insertion method,[16] in an NVT-simulation.

C. Gibbs ensemble simulations

A method that focuses specifically on the location of the liquid–vapor coexistence curve is the Gibbs–Ensemble technique.[17] Here two simulations are carried out in parallel: one in the liquid phase and one in the vapor. The two systems are held at the same temperature and are allowed to exchange volume and mass, but the total volume and total number of particles of the two systems is fixed. This ensures that, at equilibrium, the pressure and chemical potential of the two systems are the same. As a consequence, the conditions for phase coexistence are automatically satisfied. Using this technique we calculated liquid–gas coexisting densities for the case of long-range attractions ($\alpha=0.1$), where the liquid–vapor transition is stable and the phase diagram shows a critical point as well as a triple point. The coexistence data have been collected in Table I. Close to the critical point the free energy associated with the formation of the liquid–vapor interface becomes very small. As a consequence, the free energy cost to create an interface in either box becomes small, while the formation of such interfaces is entropically favorable. For this reason, just below the critical point, vapor–liquid coexistence can no longer be observed in a Gibbs Ensemble simulation.[18] Therefore the highest temperature at which the coexistence can be observed is not a proper estimate of the critical temperature of the system; nevertheless it is possible to estimate it by assuming that the temperature dependence of the density difference of the two coexisting phases can be fitted to a scaling law,[19]

$$\rho_{\mathrm{liq}}-\rho_{\mathrm{gas}}=A(T-T_c)^{\gamma}, \quad (10)$$

where γ is the critical exponent (for two dimensional systems $\gamma=0.125$), T_c is the estimate of the critical temperature, and A is a constant determined in the fit. Once T_c is known, it is possible to estimate the critical density ρ_c, by using the law of rectilinear diameters,[19]

$$\frac{\rho_{\mathrm{liq}}+\rho_{\mathrm{gas}}}{2}=\rho_c+B(T-T_c), \tag{11}$$

where B is an adjustable parameter.

IV. RESULTS

We have mapped the phase boundaries for three different ranges of attractions corresponding to $\alpha=50$, 4.5, and 0.1. Our results are summarized in Fig. 5. The first point to note is that we find clear evidence of a *first order* transition between the solid and fluid phase at finite temperatures. This finding would be trivial in three dimensions but not in two. In fact there is considerable evidence that melting in two dimensions may be a continuous phase transition.[20,21] On the other hand evidence for first order two-dimensional melting has also been observed in a number of systems[22] and there is, in fact, no theoretical reason to rule out first-order melting in two dimensions.

A. Short-range

In the first panel of Fig. 5 we show the calculated phase diagram for the shortest range considered. A relatively small system size of $N=256$ particles was used in the mapping of the phase boundary using two parallel NPT-simulations combined into the Gibbs–Duhem method. In order to shorten simulation times we have truncated, but not shifted, the potential at $r=3.5\sigma$, and maintained a neighbor list of particles within a radius of $r=5.0\sigma$. In order to prevent the solid system from melting and the liquid from crystallizing, we have used the artificial constraint on a crystallinity order parameter (see Sec. III). However, we also ran a few simulations without this artificial constraint and we verified that the phase coexistence was not an artifact due to the constraint. We performed two sets of integrations, one where we increased β stepwise (empty circles in the figure), and one in the opposite sense (filled circles). An independent evaluation of the crystallization boundary was obtained with thermodynamic integration. The squares in the figure represent the calculated coexisting densities, and are connected with a simple fitting function which is only meant to be a guide to the eye. Note that the curves for increasing and decreasing β do not superimpose everywhere. This is due to the limited numerical accuracy of our Gibbs–Duhem integration.

It is interesting to compare our results with the phase diagram calculated for particles interacting through the same potential and with same range,[23] but in *three* dimensions. Constraining the system to two dimensions causes the ''shoulder'' in the crystallization curve to become flatter and to move to lower temperatures. The latter effect is not surprising as there are more neighbors in $d=3$ than in $d=2$. For instance, a sphere in a $d=2$ close-packed structure has 6 neighbors and in $d=3$, 12 neighbors. All other things being equal, in three dimensions the freezing temperature is raised by a factor proportional to the number of neighbors. Next, the effect of thermal fluctuations increases as the dimensionality of the system is reduced. In $d=1$, solids can not exist because of thermal fluctuations. In $d=2$, there is no true long-range positional order, although there is a phase transition separating the liquid and the crystalline phase. We should expect that, due to the stronger fluctuations in two dimensional fluids, the (metastable) liquid–vapor critical temperature, T_c, should be reduced compared to the corresponding three-dimensional model.

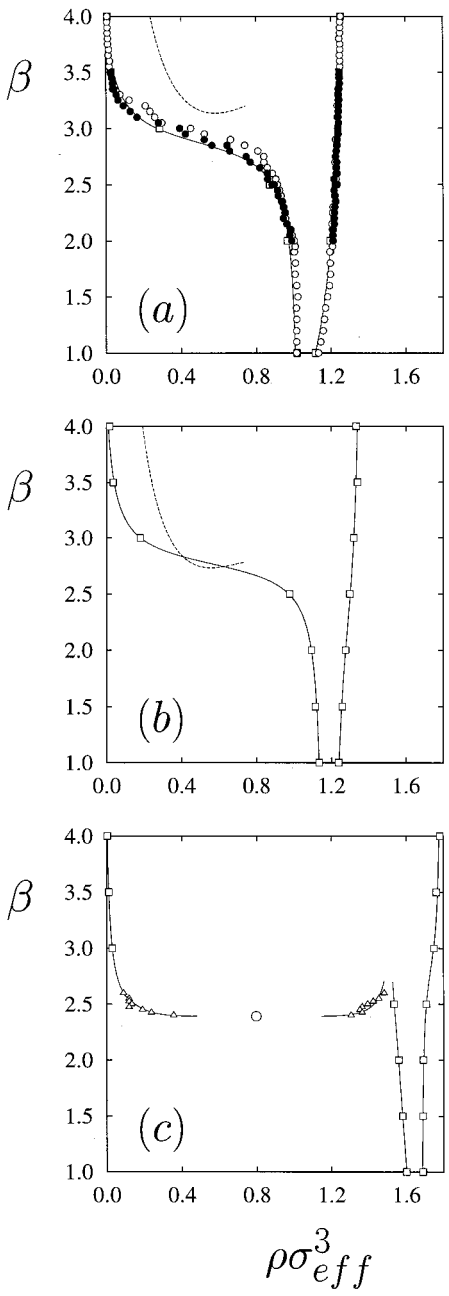

FIG. 5. Phase diagrams in the (β,ρ) representation, shown for increasing range of attractions: (a) $\alpha=0.1$, (b) $\alpha=4.5$, and (c) $\alpha=0.1$. The circles refer to the Gibbs–Duhem integration method. Here we show (○) a series for increasing β (decreasing temperature) and (●) a series for decreasing β. The squares (□) are the result of thermodynamic integration, and the line just a guide to the eye. The fluid–fluid equilibrium densities are calculated with Gibbs ensemble simulations (△) when possible, otherwise we estimated the spinodal (---) extrapolating the isothermal compressibility. See text for details.

We have attempted to locate the metastable fluid-fluid equilibrium by performing Gibbs-Ensemble simulations in the region where we estimated demixing of the metastable fluid phase to occur. However, in these simulations we saw

no fluid-fluid demixing. Rather, we noticed a strong tendency towards spontaneous crystallization. This behavior is in contrast with analogous calculations in the corresponding three-dimensional system.[23] We argue that in two dimensions the local hexagonal structure of the dense fluid, is similar to that of the solid. Only small density fluctuations are necessary to overcome a (presumably) small free energy barrier for the formation of the critical nucleus. Nevertheless we can still provide an estimate of the fluid–fluid metastable equilibrium by extrapolating to the temperature where the inverse isothermal compressibility, $\kappa^{-1}=-V(\partial P/\partial V)_T$, of the liquid phase vanishes. This is straightforward, since the equation of state of the liquid is known for several temperatures from the thermodynamic integration procedures. See, for example, Fig. 4. The inverse isothermal compressibility can be rewritten as

$$\beta\kappa^{-1}=\rho\left(\frac{\partial\beta P}{\partial\rho}\right)_T. \tag{12}$$

We assumed that the inverse compressibility depends linearly on temperature (this is not true close to the critical point, but there we have no data anyway). The set of points where the extrapolated $\beta\kappa^{-1}$ vanishes, provides us with our estimate of the metastable liquid–vapor spinodal. This estimate is shown as a dotted curve in Fig. 5.

B. Intermediate-range

We used thermodynamic integration to map out the solid–liquid equilibrium for longer range of attractions. Even though the calculation is limited to a few selected temperatures, this method has the advantage that it is more robust than the Gibbs–Duhem. The curve connecting the squares in Fig. 5 is only a guide to the eye. As we increase the range of attractions, we expect the metastable critical point to move to higher temperatures. Indeed our estimate of the critical point, obtained using the extrapolation method described above, predicts that, for the intermediate range ($\alpha=4.5$), the spinodal just about touches the crystallization boundary. We attempted to perform Gibbs ensemble simulations to study the liquid–vapor transition in this model system, but again we encountered a strong tendency of the dense phase to crystallize.

C. Long-range

The situation changes quite dramatically when the range of attraction is increased even more. The liquid–gas transition becomes stable and Gibbs-Ensemble simulations are successful in locating the phase boundaries. In Table I we collect the coexistence densities as a function of the inverse temperature. The uncertainties $\Delta\rho$ quoted in the table are not the errors in the average densities, rather they refer to the half-width of the histogram indicating the probability of finding a certain density during the simulation. By fitting the liquid and gas densities to the law of rectilinear diameters, we extrapolate the critical point at $T_c=0.418$ and $\rho_c=0.134$. The fitting curve is portrayed in the third panel of Fig. 5. The open circles are the Gibbs-Ensemble simulation coexistence densities for the liquid–gas equilibrium, while the open squares refer to the solid-fluid equilibrium and were determined through thermodynamic integration. At very low temperatures, though, calculating the fluid branch of the equation of state becomes quite a difficult task, because equilibration times become increasingly longer. Here we have estimated the crystallization boundary by Grand-Canonical (μVT) simulations of very low density systems.

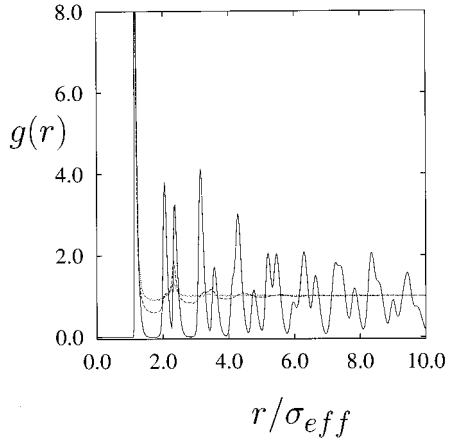

FIG. 6. Pair correlation function *g(r)* calculated in the short-range attraction $\alpha=50$ system at $T^*=2.5$ for different densities: (---) typical gas density $\rho^*=0.13$, (– – –) liquid system exactly at equilibrium $\rho^*=0.5680$, and (—) the corresponding coexisting solid system $\rho^*=0.8267$.

D. Structural properties

In order to investigate the structural properties of the phases identified in the previous sections, we have performed simulations on a larger system of 450 particles, at a single temperature, for the case of a short-range potential. The use of this larger system enables the calculation of the pair distribution functions for large separation: this is especially important in order to study the decay of the bond-order parameter close to the solid–liquid transition. Monte Carlo simulations were performed in the NPT-ensemble. The structures of the two coexisting phase were characterized using the radial distribution function *g(r)* (see Fig. 6) and the bond-order correlation function $g_6(r)$, which correlates over the value of the *local* bond-orientational order parameter ψ_6 between two particles. This is defined by

$$g_6(r)=\frac{\langle\psi_6^*(\mathbf{r}_j)\psi_6(\mathbf{r}_i)\rangle}{g(r)}, \tag{13}$$

where the local bond orientational order for particle i at a position $\mathbf{r}_i$ is given by

$$\psi_6(\mathbf{r}_i)=\frac{\Sigma_k w(r_{ik})\exp(6i\theta_{ik}))}{\Sigma_k w(r_{ik})}. \tag{14}$$

In this expression the summation is over the neighboring particles k of particle i and θ_{ik} is the angle between the vector $(\mathbf{r}_i-\mathbf{r}_k)$ and a fixed reference axis. We used a weighting function w to define nearest neighbors.[24] In the present study, we chose *w(r)* such that it is unity for a separation of $r<1.6\sigma$ and zero for r_{ik} above 1.8σ with a linear interpolation between the two endpoints. The upper limit of the

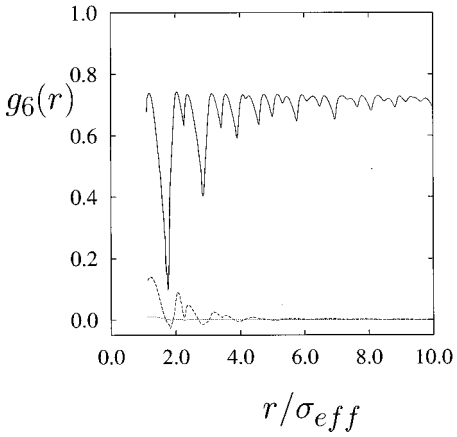

FIG. 7. The bond orientational correlation function $g_6(r)$ calculated for the systems described in Fig. 6. Note how the low density system carries no bond correlations even at short distances; the correlation in the liquid is lost within 4–5 particle diameters, but in the solid the bond-order parameter tends to a nonzero value in the limit of long particle–particle separation.

weighting function was chosen such that all the particles included in the first peak of the pair distribution function contribute to ψ_6. The bond-order correlation function is large if local bond-order parameters are correlated over large distances (as they are in the crystalline solid). In the isotropic liquid, bond-order correlation decay exponentially. However, in the hexatic phase, an algebraic decay is expected. Our results for $g_6(r)$ are shown in Fig. 7; it is apparent that $g_6(r)$ rapidly tends to zero in the liquid phase, and therefore the liquid phase at coexistence is not even close to becoming hexatic. Of course, in the coexisting solid phase, the bond orientational correlation function tends to a nonzero value, as it should. These findings support our ''thermodynamic'' observation that the fluid–solid transition in these model system appears to be first order.

V. CONCLUSIONS

We have studied the phase behavior of simple model system that is meant to mimic membrane proteins confined in a quasi-two-dimensional geometry. To study the phase behavior, we used a variety of complementary simulation techniques. Where possible we have used various routes to estimate the phase boundaries. Our study focused on the influence of the range of the attractive interactions on the topology of the phase diagram. For long-ranged attractions the phase diagram displays a stable liquid–vapor critical point and a solid–liquid–vapor triple point. As the range of attraction is decreased, the stable liquid–gas transition becomes metastable and the critical point moves into the solid-fluid two-phase region. Qualitatively, the phase diagrams of the two-dimensional systems that we studied are similar to those of their three-dimensional counterparts. However, quantitatively, there are large differences. Most importantly, we find that in systems where the liquid–vapor coexistence curve has moved below the freezing curve, there is virtually no barrier to crystallization. This suggests that membrane proteins with effectively isotropic interactions should easily form two-dimensional crystals. Two questions arise: (1) how do these two dimensional crystals proceed to form three-dimensional crystals; and (2) to what extent is the ease of 2*d* crystallization changed by anisotropy in the protein–protein interactions?

ACKNOWLEDGMENTS

The work of the FOM Institute is part of the research program of ''Stichting Fundamenteel Onderzoek der Materie'' (FOM) and is supported by NWO. Computing time was provided by SARA (Stichting Academisch Rekencentrum Amsterdam). The authors gratefully acknowledge Martin Bates for useful discussions and for helping with the details of the simulations. The authors also thank Anand Yethiraj and Jurgen Horbach for critical reading of the paper. M.G.N. acknowledges financial support from EU Contract No. ERBFM-BICT982949.

[1] A. McPherson, *Preparation and Analysis of Protein Crystals* (Krieger, Malabar, 1982).
[2] S. D. Durbin and F. Feher, Annu. Rev. Phys. Chem. **47**, 171 (1996).
[3] D. Rosenbaum, P. C. Zamora, and C. F. Zukoski, Phys. Rev. Lett. **76**, 150 (1996); A. George and W. Wilson, Acta Crystallogr., Sect. D: Biol. Crystallogr. **50**, 361 (1994).
[4] M. Hagen and D. Frenkel, J. Chem. Phys. **101**, 4093 (1994).
[5] H. C. Andersen, J. D. Weeks, and D. Chandler, Phys. Rev. A **4**, 1579 (1971).
[6] J. A. Barker and D. Henderson, Rev. Mod. Phys. **48**, 587 (1976).
[7] D. A. Kofke, Mol. Phys. **78**, 1331 (1993).
[8] D. A. Kofke, J. Chem. Phys. **98**, 4149 (1993).
[9] A. Jaster, Phys. Rev. E **59**, 2594 (1999).
[10] M. A. Bates and D. Frenkel, Phys. Rev. E **61**, 5223 (2000).
[11] P. J. Steinhardt, D. R. Nelson, and M. Ronchetti, Phys. Rev. B **28**, 784 (1983).
[12] B. Barboy and W. M. Gelbart, J. Chem. Phys. **71**, 3053 (1979).
[13] D. Frenkel and A. J. C. Ladd, J. Chem. Phys. **81**, 3188 (1984).
[14] J. M. Polson, E. Trizac, S. Pronk, and D. Frenkel, J. Chem. Phys. **112**, 5339 (2000).
[15] D. Frenkel and B. Smit, *Understanding Molecular Simulations* (Academic, New York, 1996).
[16] B. Widom, J. Chem. Phys. **39**, 2802 (1963).
[17] A. Z. Panagiotopoulos, Mol. Phys. **61**, 813 (1087).
[18] B. Smit, Ph. de Smedt, and D. Frenkel, Mol. Phys. **68**, 931 (1989).
[19] J. S. Rowlinson and B. Widom, *Molecular Theory of Capillarity* (Clarendon, Oxford, 1982).
[20] See, for example, C. A. Murray and D. H. van Winkle, Phys. Rev. Lett. **58**, 1200 (1987); R. E. Kusner, J. A. Mann, J. Kerins, and A. J. Dahm, *ibid.* **73**, 3113 (1994); A. H. Marcus and S. A. Rice, *ibid.* **77**, 2577 (1996); K. Zahn, R. Lenke, and G. Maret, *ibid.* **82**, 2721 (1999).
[21] See, for example, B. J. Alder and T. E. Wainwright, Phys. Rev. **127**, 359 (1962); K. J. Strandburg, J. A. Zollweg, and G. V. Chester, Phys. Rev. B **30**, 2755 (1984); K. W. Wojchiechiwski and A. C. Branka, Phys. Lett. A **134**, 314 (1988); K. Bagchi, H. C. Andersen, and W. Swope, Phys. Rev. E **53**, 3794 (1996); A. Jaseter, *ibid.* **59**, 2594 (1999).
[22] D. Andelman, F. Brochard, C. Knobler, and E. Rondelez, in *Micelles, Membranes, Microemulsions and Monolayers*, edited by W. M. Gelbart, A. Ben-Shaul, and D. Roux (Springer-Verlag, New York, 1994).
[23] P. R. ten Wolde and D. Frenkel, Science **277**, 1975 (1997).
[24] K. L. Strandberg, *Bond Orientational Order in Condensed Matter Systems* (Springer-Verlag, New York, 1992).